Article

Not peer-reviewed version

Probing Chirality of the Quantum Hall Effect via the Landauer-Büttiker Formalism with Two Current Sources

Kyung Ho Kim *

Posted Date: 13 August 2025

doi: 10.20944/preprints202508.0930.v1

Keywords: quantum Hall effect; edge states; topological protection; linear superposition; Landauer-Büttiker formalism; two current sources

 doi:10.20944/preprints202508.0930.v1

Article

Probing Chirality of the Quantum Hall Effect via the Landauer-Büttiker Formalism with Two Current Sources

Kyung Ho Kim

Department of physics and Astronomy, Sejong University, Seoul 05006, Republic of Korea;
kyungho@sejong.ac.kr

Abstract

The quantum Hall effect is a paradigmatic example of topological order, characterized by precisely quantized Hall resistance and dissipationless edge transport. These edge states are chiral, propagating unidirectionally along the boundary, and their directionality is determined by the external magnetic field. While chirality is a central feature of the quantum Hall effect, directly probing it remains experimentally nontrivial. In this study, we introduce a simple and effective method to probe the chirality of edge transport using two independently controlled current sources in a Hall bar geometry. The system under investigation is a monolayer epitaxial graphene grown on a silicon carbide substrate, exhibiting robust quantum Hall states. By varying the configurations of the two current sources, we measure terminal voltages and analyze the transport characteristics. Our results demonstrate that the observed behavior can be understood as a linear superposition of chiral contributions to the edge transport. This superposition enables tunable combinations of longitudinal and Hall resistances and enables additive or canceling behavior of Hall voltages depending on current source configuration. The Landauer-Büttiker formalism provides a quantitative framework to describe these observations, capturing the interplay between edge state chirality and the measurement configuration. This research offers a simple yet effective experimental and analytical approach for probing chiral edge currents and highlights the linear superposition principle in the quantum Hall effect.

Keywords: quantum Hall effect; edge states; topological protection; linear superposition; Landauer-Büttiker formalism; two current sources

MSC: 00A79

1. Introduction

The quantum Hall effect (QHE) is characterized by the precise quantization of Hall resistance and the vanishing of longitudinal resistance in the presence of a strong perpendicular magnetic field [1]. Depending on the system, the quantized values can correspond to integer [2], half-integer [3], or fractional multiples of the fundamental resistance quantum [4]. This quantization arises from the formation of topologically non-trivial insulating bulk states, which give rise to robust and dissipationless edge channels [5–8]. These topological features are believed to ensure the robustness and precision of quantized transport [9,10] and serve as the foundation for related phenomena such as the quantum anomalous Hall effect [11] and the quantum spin Hall effect [12], which can occur even in the absence of an external magnetic field. The exactness of quantized Hall resistance has enabled its use in applications such as quantum resistance standards and electrical metrology [9,10].

One of the defining features of QHE is the presence of chiral edge currents coexisting with an insulating bulk [1]. Classically, this behavior can be understood as arising from skipping cyclotron

 doi:10.20944/preprints202508.0930.v1

orbits along the sample boundaries [13]. Quantum mechanically, it originates from the formation of discrete Landau levels and their bending near the sample edge [13]. From a topological perspective, edge states arise from the bulk–edge correspondence [5–8]. The existence of chiral edge states and an insulating interior has been investigated through local probe techniques [14,15] and noise measurements [16,17]. This unique transport phenomenon has motivated the exploration of the QHE in a variety of geometries, including three-dimensional structures [18], series and parallel connections [19], and anti-Hall bar or Corbino type configurations [20–26]. The QHE remains at research frontier, with topics including the incompressible nature of the bulk [27], the appearance of hot spots [28], and the intriguing behavior of snake states [29].

In this work, we investigate the chirality of edge states in QHE using two current source (TCS) excitations in a standard Hall bar geometry. The use of TCS enables a variety of excitation and measurement configurations, offering new approaches to probing the chirality of edge currents generated by each source. All measurements across different configurations are analyzed using the Landauer-Büttiker formalism (LBF) [30,31]. The results are consistent with the presence of chiral edge currents and a bulk that remains incompressible: the total current contributed by each source flows in the same direction regardless of the configuration. This behavior contrasts sharply with that of conventional diffusive conductors, where oppositely directed currents would be expected to partially or fully cancel. The TCS-based method thus provides compelling additional evidence for the chiral nature of edge states in the QHE.

2. Materials and Methods

For this study, we used monolayer epitaxial graphene (epigraphene) grown on silicon carbide substrates as the two-dimensional channel [9,10]. The epigraphene was patterned into a Hall bar geometry (**Figure 1**(a), width = 30 μm, length = 180 μm) using electron-beam lithography and was doped near the charge neutrality point (~5 × 10^{10} electrons/cm²) through a molecular doping method (See **Figure 1**(f)) [32]. This low carrier density enables high mobility, resulting in a robust QHE. After doping, the sample exhibited a carrier mobility of 32,000 cm²/V·s and a sheet resistance of 4 kΩ/□ at a temperature of 2 K. A perpendicular magnetic field was applied to the sample surface to induce a QH state with a filling factor of ν = 2, corresponding to the first plateau in the half-integer QHE of epigraphene [3]. All measurements were performed at T = 2 K using two Keithley current sources and nanovoltmeters.

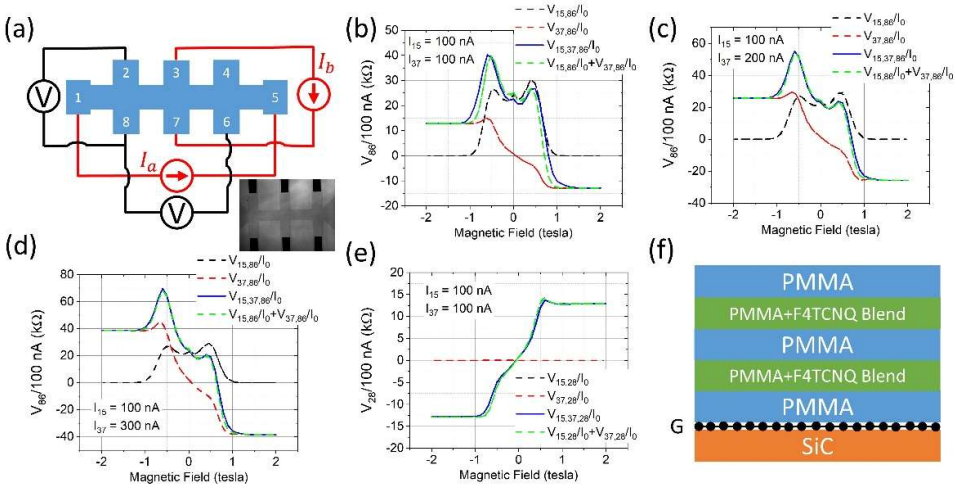

Figure 1. (a) Measurement configuration with two current sources in a Hall bar geometry. (b-d) Voltage between terminals 8 and 6 measured for different current combinations: (b) $I_a = 100$ nA, $I_b = 100$ nA; (c), $I_a = 100$ nA , $I_b = 200$ nA (d), $I_a = 100$ nA, $I_b = 300$ nA. (e) Voltage between terminals 2 and 8 for $I_a = 100$ nA, $I_b = 100$

 doi:10.20944/preprints202508.0930.v1

nA. I_0 = 100 nA denotes the reference current unit. (f) Schematic of the molecular doping, showing multiple layers of poly(methyl methacrylate) (PMMA) and a PMMA+ 2,3,5,6-Tetrafluoro-tetracyano-quino-dimethane (F4TCNQ) blend on top of the epitaxial graphene.

Before performing the main measurements, we evaluated the contact resistances of all eight terminals on the sample using the three-terminal method under quantum Hall conditions [33]. In the three-terminal method, contact resistance is estimated by measuring the longitudinal resistance with one of the voltage probes placed on the drain contact. Then the measured resistance is the sum of the contact resistance of the drain contact and the lead resistance. All contact resistances were found to be below 10 Ω, except for contact 2 (Rc = 60 Ω), contact 7 (Rc = 60 Ω), and contact 8 (Rc = 40 kΩ) (see **Figure 1** for contact numbering). The carrier density extracted from the Hall voltage measured between terminals 2 and 8 was 3.5 × 10¹⁰ electrons/cm², which deviates from the values obtained using other voltage probes (e.g., terminals 3–7 and 4–6), where the carrier density was approximately 5 × 10¹⁰ electrons/cm². This discrepancy could be related to the high contact resistance of terminal 8. For the carrier density measurements, current was sourced through contacts 1 and 5. The robustness of the QHE in our sample is further confirmed by the observation of a critical current as high as 5 μA at a magnetic field of 2 T and a temperature of 2 K.

3. Results

Figure 1(a) shows a schematic of the TCS configuration, where the current source A and B supply currents I_a and I_b, which are directed horizontally and vertically, respectively. The voltage measured between terminals 8 and 6 when both current sources are active ($I_a = I_{15}$, $I_b = I_{37}$) is denoted by $V_{15,37,86}$. Due to the chirality of the edge currents in the QH regime, we expect that the principle of superposition to hold in the TCS configuration: the voltage when both current sources are on should equal the sum of the voltages measured when each source is applied individually. To test this, we compare $V_{15,37,86}$ with $V_{15,86} = I_{15}R_{15,86}$ and $V_{37,86} = I_{37}R_{37,86}$, where each is measured with the other current source turned off. As shown in *Figure 1*(b) we find that $V_{15,37,86} = V_{15,86} + V_{37,86}$, consistent with the quantized Hall resistance $R = h/2e^2$ or zero in the QH state. We further verify this superposition behavior by fixing I_{15} = 100 nA and varying I_{37} as 100 nA, 200 nA, 300 nA. The resulting voltage $V_{15,37,86}$ changes accordingly, with $V_{15,86}$ remaining constant and $V_{37,86}$ varying linearly, as expected (*Figure 1*(c,d)). The superposition principle is also confirmed at another voltage terminal pair: $V_{15,37,28} = V_{15,28} + V_{37,28}$, where $V_{15,28} = I_{15} \cdot (h/2e^2)$ in the QH regime with $\nu = 2$ as shown in *Figure 1*(e).

We explain the linear superposition behavior observed in the QHE with TCS as shown in *Figure 1* using the LBF. In the QH regime at filling factor $\nu = 2$, the LBF accounts for chiral edge channels that contribute a quantum conductance of $2e^2/h$, while the bulk remains incompressible. This quantization $2e^2/h$ arises from the half integer QH effect in monolayer graphene, where the Hall conductivity is given by $\sigma_{xy} = g(N + \frac{1}{2})e^2/h$ with degeneracy $g = 4$ reflecting the spin and valley degeneracy, and the zeroth Landau level ($N = 0$) [3]. Within the LBF framework, the current and voltage at each terminal can be expressed as:

$$I_i = (2e^2/h)\sum_j \left(T_{ji}V_i - T_{ij}V_j\right) = (2e^2/h)\,(V_i - V_{i-1}) \quad \text{(Eq. 1)}$$

Here, I_i denotes the current flowing out of ith terminal into the sample, V_i is the voltage at the ith terminal, and T_{ji} is the transmission probability for an electron injected from terminal i to reach terminal j. Charge conservation requires $\sum_i I_i = 0$. For dissipationless chiral transport in the QH regime, the transmission probabilities are defined as $T_{ji} = 1$ if $j = i + 1$ and $T_{ji} = 0$ otherwise [30,31]. When both current sources on, LBF allows linear superposition:

$$I_i^{(a,b)} = I_i^{(a)} + I_i^{(b)},\ V_i^{(a,b)} = V_i^{(a)} + V_i^{(b)}, \quad \text{(Eq. 2)}$$

where $I_i^{(a,b)}$ and $V_i^{(a,b)}$ are the total current and voltage at terminal i with both sources are on, and $I_i^{(a)}$, $V_i^{(a)}$ (respectively $I_i^{(b)}$, $V_i^{(b)}$) are those when only source a (respectively b) is on. In the specific configuration shown in *Figure* 1, where $I_a = I_{15}$ and $I_b = I_{37}$, the LBF gives:

$$I_1^{(a)} = I_a = -I_5^{(a)},\ I_3^{(b)} = I_b = -I_7^{(b)},$$

 doi:10.20944/preprints202508.0930.v1

with zero currents at all other terminals. For the voltages, we find:

$V_i^{(a)} = V_1^{(a)} = V_a$ for $i = 1,2,3,4$, $V_i^{(b)} = V_3^{(b)} = V_b$ for $i = 3,4,5,6$

and zero for other terminals. From this, we obtain:

$V_8^{(a,b)} - V_6^{(a,b)} = -V_3^{(b)} = -V_b = -(h/2e^2)\, I_b$, $V_2^{(a,b)} - V_8^{(a,b)} = V_1^{(a)} = V_a = (h/2e^2)\, I_a$. Each voltage drop is determined solely by the corresponding current source. These results are in excellent agreement with the experimental observations in *Figure 1*(b-e).

We investigate additional configurations and conclude that QHE with TCS consistently follows the additive nature of the LBF, regardless of the configuration. In *Figure 2*, the positions of the current sources are fixed as in *Figure 1*, but the voltage is measured between terminal 2 and 6. In this set up, both $V_{15,26}$ and $V_{37,26}$ contain contributions from both longitudinal and transverse conductance arising from current I_a and I_b, respectively. According to the LBF, the superposition of contributions from both sources predicts:

$V_2^{(a,b)} - V_6^{(a,b)} = V_a - V_b = (h/2e^2)\,(I_a - I_b)$,

indicating that both currents contribute to the Hall voltage. This prediction is verified in *Figure 2*. In *Figure 2*(b), the Hall voltage is completely canceled when $I_a = I_b$, consistent with the expected result. Figure 2(c) and 2(d) demonstrate that the Hall voltages can be tuned and made asymmetric by varying the relative magnitudes of the two current sources.

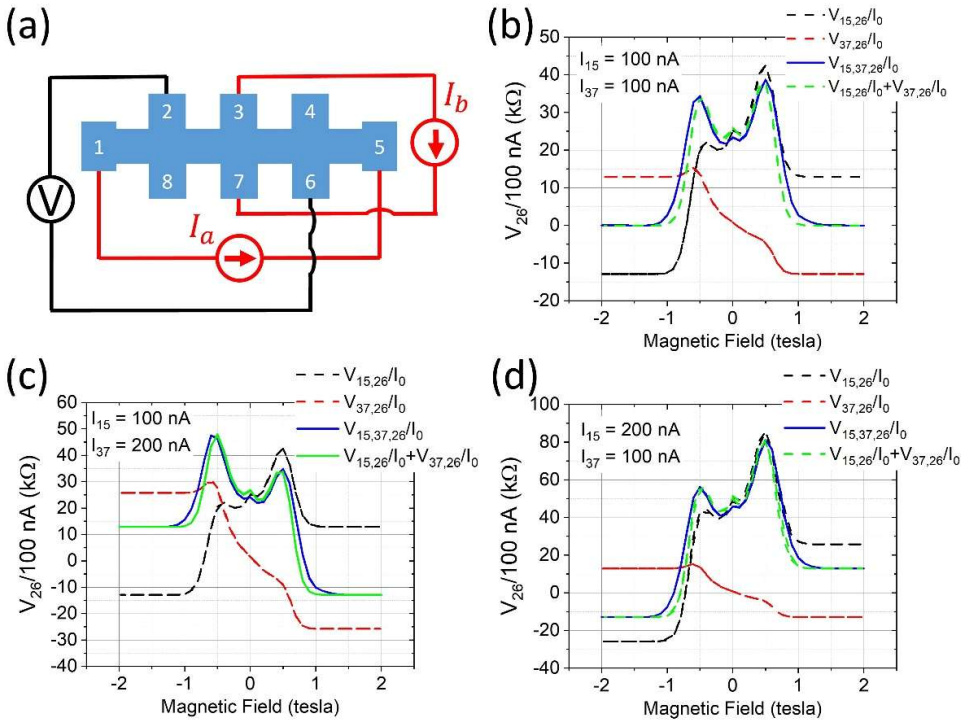

Figure 2. (a) Measurement configuration with two current sources. (b-d) Voltage between terminals 2 and 6 measured under different conditions: (b) $I_a = 100$ nA, $I_b = 100$ nA (c) $I_a = 100$ nA, $I_b = 200$ nA (d) $I_a = 200$ nA, $I_b = 100$ nA. The reference current $I_0 = 100$ nA.

In Figure 3, we explore configurations where the two current sources I_a and I_b are applied parallel (*Figure 3*(a)) and antiparallel (*Figure 3*(d)) directions, such that the current either add or cancel. According to the LBF, for the parallel configuration in *Figure* 3(a), the currents are distributed as:

$I_1^{(a)} = I_a = -I_5^{(a)}$, $I_2^{(b)} = I_b = -I_4^{(b)}$,

with zero currents at all other terminals. The corresponding voltages are:

$V_i^{(a)} = V_1^{(a)} = V_a$ for $i = 1,2,3,4$, and $V_i^{(b)} = V_2^{(b)} = V_b$ for $i = 2,3$

 doi:10.20944/preprints202508.0930.v1

; the other terminals have zero voltage. In this configuration, the expected voltage differences are:

$V_8^{(a,b)} - V_6^{(a,b)} = 0,\ V_3^{(a,b)} - V_7^{(a,b)} = V_a + V_b = (h/2e^2)\,(I_a + I_b).$

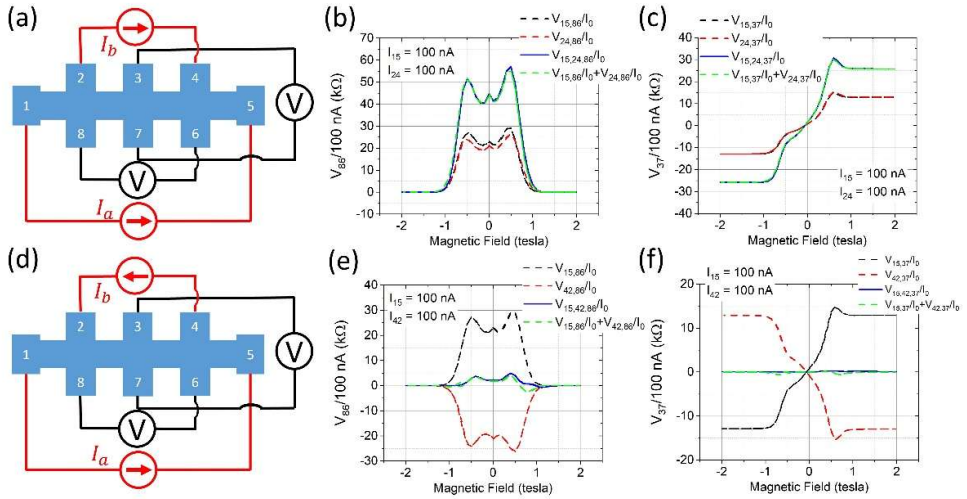

Figure 3. (a) Measurement configuration for the parallel injection case, corresponding to panels (b) and (c). (b) Voltage between terminals 8 and 6 measured with $I_a = 100$ nA and $I_b = 100$ nA. (c) Voltage between terminals 3 and 7 under the same parallel current conditions. (d) Measurement configuration for the antiparallel current injection case, corresponding to panels (e) and (f). (e) Voltage between terminals 8 and 6 with $I_a = 100$ nA and $I_b = 100$ nA. (f) Voltage between terminals 3 and 7 under the same antiparallel conditions. The reference current $I_0 = 100$ nA.

The experimental results in *Figure 3*(b) and (c) confirm these predictions.

In the antiparallel configuration shown in *Figure 3*d, only the direction of current for source B is reversed.

$I_4^{(b)} = I_b = -I_2^{(b)}$ and $V_i^{(b)} = V_2^{(b)} = V_b$ for $i = 4,5,6,7,8,1$

; voltages at the other terminals remain zero. The resulting voltage differences are:

$V_8^{(a,b)} - V_6^{(a,b)} = V_b - V_b = 0$ and $V_3^{(a,b)} - V_7^{(a,b)} = V_a - V_b = (h/2e^2)\,(I_a - I_b)$

, which are in excellent agreement with the experimental data shown in *Figure 3*(e) and (f). These results clearly demonstrate that even when I_b is applied from terminal 4 to terminal 2 in the antiparallel configuration, the current does not flow directly from the short path 4→3→2. Instead, due to the chirality of the edge states, it follows a longer clockwise path: 4→5→6→7→8→1→2.

We further examine a configuration in which the two current sources share a common drain contact, as shown in *Figure 4*. According to the LBF, the current distribution in this setup is $I_1^{(a)} = I_a = -I_4^{(a)}$, $I_8^{(b)} = I_b = -I_4^{(b)}$, with zero currents at all other terminals. The corresponding voltages are $V_i^{(a)} = V_1^{(a)} = V_a$ for terminals $i = 1,2,3$ and $V_i^{(b)} = V_8^{(b)} = V_b$ for $i = 8,1,2,3$. All other terminals have zero voltages. From this, we find the following voltage differences:

$V_2^{(a,b)} - V_3^{(a,b)} = (V_a + V_b) - (V_a + V_b) = 0,$

$V_2^{(a,b)} - V_7^{(a,b)} = V_a + V_b = (h/2e^2)\,(I_a + I_b).$

These predictions are in excellent agreement with the experimental results shown in *Figure 4*(b) and *Figure 4*(c).

 doi:10.20944/preprints202508.0930.v1

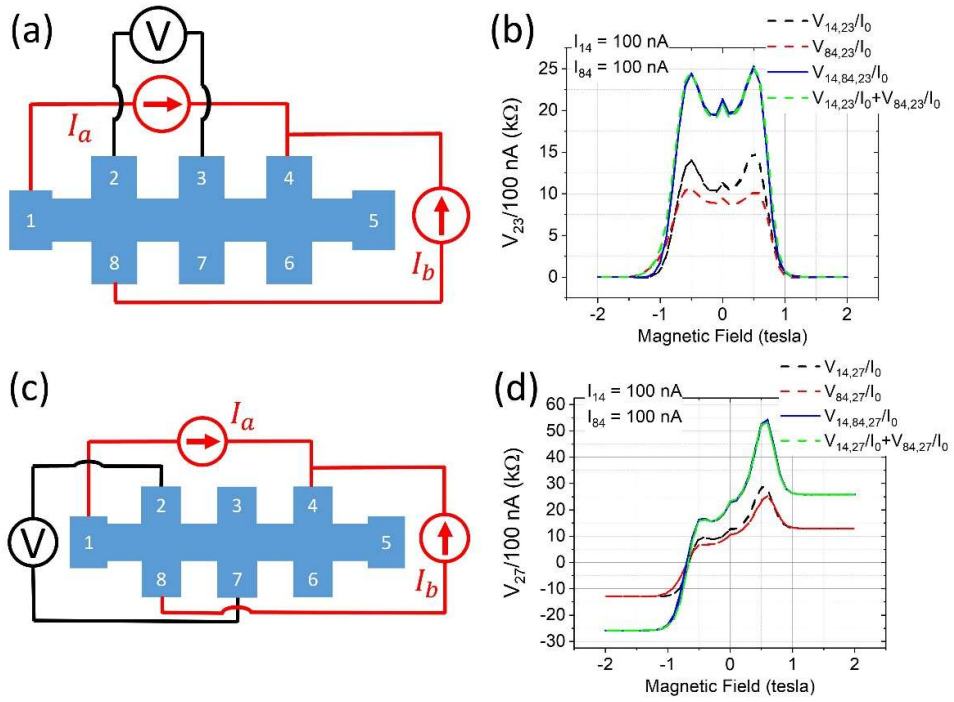

Figure 4. Measurement configuration where two current sources share a common drain. (a) Setup corresponding to the measurement shown in (b). (b) Voltage between terminals 2 and 3 with I_a =100 nA and I_b =100 nA. (c) Setup corresponding to the measurement shown in (d). (d) Voltage between terminals 2 and 7 with I_a =100 nA and I_b =100 nA. The reference current I_0 =100 nA.

4. Discussion

We explored additional current source configurations and confirmed that the LBF consistently describes transport behavior in all cases. The chiral edge currents along the sample boundary are schematically illustrated in **Figure 5** for a configuration where $\boldsymbol{I_a}$ and $\boldsymbol{I_b}$ are nominally applied in opposite directions. Unlike in conventional conductors, where opposing currents may cancel each other, the zero quantum Hall voltages observed in **Figure 3**(e) and 3(f) do not result from vanishing net current. Instead, they arise from the specific voltage distribution dictated by chiral edge transport, as described by Eq. (1).

 doi:10.20944/preprints202508.0930.v1

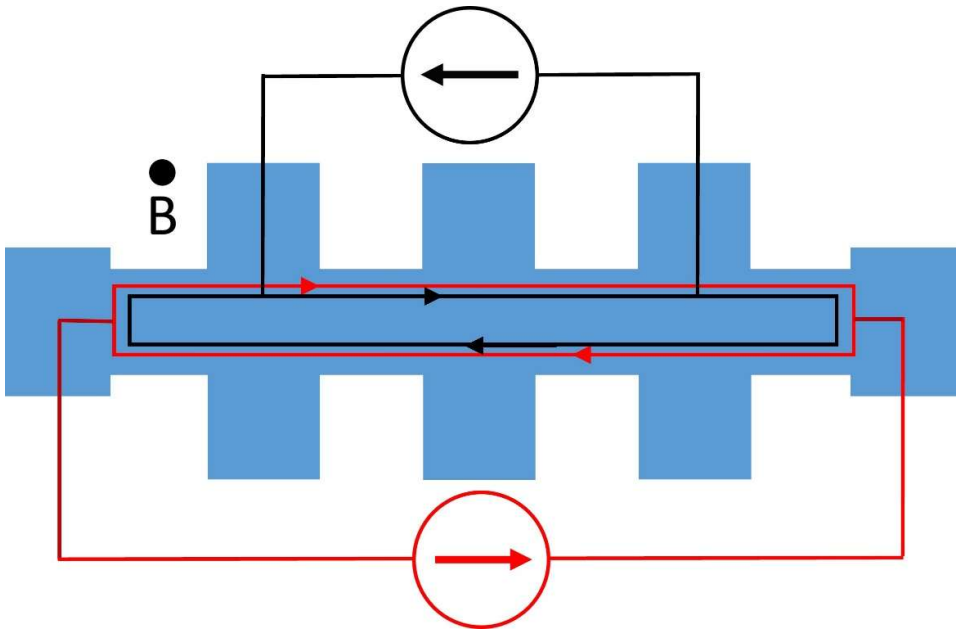

Figure 5. Schematic of current distribution in multiple current source excitation configuration. Each current from the respective source follows the same chiral edge direction, resulting in the additive behavior of the QHE.

5. Conclusions

We have experimentally demonstrated the linear superposition principle of QH transport under TCS excitations in a conventional Hall bar geometry. Our device is based on epitaxial monolayer graphene, doped near the charge neutrality point to enhance mobility and stabilize the QH state. The observed superposition reveals a combinatorial transport behavior in which both longitudinal and transverse QH resistances coexist in a tunable way. This TCS-based approach provides a powerful and flexible method for probing chirality and edge transport in QH systems.

Funding: This work was jointly supported by the IITP under Grant No. RS-2024-00437191, funded by the Ministry of Science and ICT (MSIT), Korea, the faculty research fund of Sejong University in 2025, and the Korean-Swedish Basic Research Cooperative Program of the NRF (No. NRF-2017R1A2A1A18070721), and the Swedish Foundation for Strategic Research (SSF) (No. IS14-0053, GMT14-0077, and RMA15-0024).

Data Availability Statement: We encourage all authors of articles published in MDPI journals to share their research data. In this section, please provide details regarding where data supporting reported results can be found, including links to publicly archived datasets analyzed or generated during the study. Where no new data were created, or where data is unavailable due to privacy or ethical restrictions, a statement is still required. Suggested Data Availability Statements are available in section "MDPI Research Data Policies" at https://www.mdpi.com/ethics.

Acknowledgments: K.H.K. thanks Hans He for fabricating the sample.

Conflicts of Interest: The authors declare no conflicts of interest.

Abbreviations

The following abbreviations are used in this manuscript:

QHE	Quantum Hall Effect
TCS	Two Current Sources
LBF	Landauer-Büttiker formalism
QH	Quantum Hall

 doi:10.20944/preprints202508.0930.v1

References

1. Tong, D. *Lectures on the Quantum Hall Effect*; arXiv:1606.06687, 2016.
2. von Klitzing, K.; Dorda, G.; Pepper, M. New method for high-accuracy determination of the fine-structure constant based on quantized Hall resistance. *Phys. Rev. Lett.* **1980**, *45*, 494–497. https://doi.org/10.1103/PhysRevLett.45.494.
3. Zhang, Y.; Tan, Y.-W.; Stormer, H.L.; Kim, P. Experimental observation of the quantum Hall effect and Berry's phase in graphene. *Nature* **2005**, *438*, 201–204. https://doi.org/10.1038/nature04235.
4. Stormer, H.L.; Tsui, D.C.; Gossard, A.C. The fractional quantum Hall effect. *Rev. Mod. Phys.* **1999**, *71*, S298–S305. https://doi.org/10.1103/RevModPhys.71.S298.
5. von Klitzing, K. The quantum Hall effect—An edge phenomenon? *Physica B* **1993**, *184*, 1–6. https://doi.org/10.1016/0921-4526(93)90311-S.
6. Avron, J.E.; Osadchy, D.; Seiler, R. A topological look at the quantum Hall effect. *Phys. Today* **2003**, *56*, 38–43. https://doi.org/10.1063/1.1611351.
7. Thouless, D.J.; Kohmoto, M.; Nightingale, M.P.; den Nijs, M. Quantized Hall conductance in a two-dimensional periodic potential. Phys. Rev. Lett. 1982, 49, 405–408. https://doi.org/10.1103/PhysRevLett.49.405.
8. Hatsugai, Y. Chern number and edge states in the integer quantum Hall effect. *Phys. Rev. Lett.* **1993**, *71*, 3697–3700. https://doi.org/10.1103/PhysRevLett.71.3697.
9. Tzalenchuk, A.; Lara-Avila, S.; Kalaboukhov, A.; Paolillo, S.; Syväjärvi, M.; Yakimova, R.; Kazakova, O.; Janssen, T.J.B.M.; Fal'ko, V.; Kubatkin, S. Towards a quantum resistance standard based on epitaxial graphene. *Nat. Nanotechnol.* **2010**, *5*, 186–189. https://doi.org/10.1038/nnano.2009.474.
10. He, H.; Cedergren, K.; Shetty, N.; Lara-Avila, S.; Kubatkin, S.; Bergsten, T.; Eklund, G. Accurate graphene quantum Hall arrays for the new International System of Units. *Nat. Commun.* **2022**, *13*, 6933. https://doi.org/10.1038/s41467-022-34680-0.
11. Chang, C.-Z.; et al. Colloquium: Quantum anomalous Hall effect. *Rev. Mod. Phys.* **2023**, *95*, 011002. https://doi.org/10.1103/RevModPhys.95.011002.
12. Bernevig, B.A.; Zhang, S.-C. Quantum Spin Hall Effect. *Phys. Rev. Lett.* **2006**, *96*, 106802. https://doi.org/10.1103/PhysRevLett.96.106802.
13. Haug, R.J. Edge-state transport and its experimental consequences in high magnetic fields. *Semicond. Sci. Technol.* **1993**, *8*, 131–153. https://doi.org/10.1088/0268-1242/8/2/001.
14. Ji, Z.; Park, H.; Barber, M.E.; Hu, C.; Watanabe, K.; Taniguchi, T.; Chu, J.-H.; Xu, X.; Shen, Z.-X. Local probe of bulk and edge states in a fractional Chern insulator. *Nature* **2024**, *635*, 578–583. https://doi.org/10.1038/s41586-024-08092-7.
15. Ilani, S.; Martin, J.; Teitelbaum, E.; Smet, J.H.; Mahalu, D.; Umansky, V.; Yacoby, A. The microscopic nature of localization in the quantum Hall effect. *Nature* **2004**, *427*, 328–332. https://doi.org/10.1038/nature02230.
16. de Picciotto, R.; Reznikov, M.; Heiblum, M.; Umansky, V.; Bunin, G.; Mahalu, D. Direct observation of a fractional charge. *Nature* **1997**, *389*, 162–164. https://doi.org/10.1038/38241.
17. Garg, M.; Maillet, O.; Samuelson, N.L.; Wang, T.; Feng, J.; Cohen, L.A.; Watanabe, K.; Taniguchi, T.; Roulleau, P.; Sassetti, M.; Zaletel, M.; Young, A.F.; Ferraro, D.; Roche, P.; Parmentier, F.D. Enhanced shot noise in graphene quantum point contacts with electrostatic reconstruction. *arXiv* **2025**, arXiv:2503.17209.
18. Tang, F.; Ren, Y.; Wang, P.; Zhong, R.; Schneeloch, J.; Yang, S.A.; Yang, K.; Lee, P.A.; Gu, G.; Qiao, Z.; Zhang, L. Three-dimensional quantum Hall effect and metal–insulator transition in ZrTe5. *Nature* **2019**, *569*, 537–541. https://doi.org/10.1038/s41586-019-1180-9.
19. Delahaye, F. Series and parallel connection of multiterminal quantum Hall-effect devices. *J. Appl. Phys.* **1993**, *73*, 7914–7920. https://doi.org/10.1063/1.353944.
20. Mani, R.G.; von Klitzing, K. Hall effect under null current conditions. *Appl. Phys. Lett.* **1994**, *64*, 1262–1264. https://doi.org/10.1063/1.110859.
21. Mani, R.G. Transport study of GaAs/AlGaAs heterostructure- and n-type GaAs-devices in the anti Hall bar within a Hall bar configuration. *J. Phys. Soc. Jpn.* **1996**, *65*, 1751–1759. https://doi.org/10.1143/JPSJ.65.1751.
22. Mani, R.G. Experimental technique for realizing dual and multiple Hall effects in a single specimen. *Europhys. Lett.* **1996**, *34*, 139–144. https://doi.org/10.1209/epl/i1996-00429-5.

 doi:10.20944/preprints202508.0930.v1

23. Mani, R.G. Steady-state bulk current at high magnetic fields in Corbino-type GaAs/AlGaAs heterostructure devices. *Europhys. Lett.* **1996**, *36*, 203–208. https://doi.org/10.1209/epl/i1996-00211-3.
24. Oswald, M.; Oswald, J.; Mani, R.G. Voltage and current distribution in a doubly connected two-dimensional quantum Hall system. *Phys. Rev. B* **2005**, *72*, 035334. https://doi.org/10.1103/PhysRevB.72.035334.
25. Oswald, J.; Oswald, M. Magnetotransport in a doubly connected two-dimensional quantum Hall system in the low magnetic field regime. *Phys. Rev. B* **2006**, *74*, 153315. https://doi.org/10.1103/PhysRevB.74.153315.
26. Uiberacker, C.; Stecher, C.; Oswald, J. Microscopic details of the integer quantum Hall effect in an anti-Hall bar. *Phys. Rev. B* **2012**, *86*, 045304. https://doi.org/10.1103/PhysRevB.86.045304.
27. Kendirlik, E.M.; Sirt, S.; Kalkan, S.B.; Ofek, N.; Umansky, V.; Siddiki, A. The local nature of incompressibility of quantum Hall effect. *Nat. Commun.* **2017**, *8*, 14082. https://doi.org/10.1038/ncomms14082.
28. Komiyama, S.; Sakuma, H.; Ikushima, K.; Hirakawa, K. Electron temperature of hot spots in quantum Hall conductors. *Phys. Rev. B* **2006**, *73*, 045333. https://doi.org/10.1103/PhysRevB.73.045333.
29. Rickhaus, P.; Makk, P.; Liu, M.-H.; Tóvári, E.; Weiss, M.; Maurand, R.; Richter, K.; Schönenberger, C. Snake trajectories in ultraclean graphene p–n junctions. *Nat. Commun.* **2015**, *6*, 6470. https://doi.org/10.1038/ncomms7470.
30. Büttiker, M. Absence of backscattering in the quantum Hall effect in multiprobe conductors. *Phys. Rev. B* **1988**, *38*, 9375–9389. https://doi.org/10.1103/PhysRevB.38.9375.
31. Datta, S. *Electronic Transport in Mesoscopic Systems*; Cambridge University Press: Cambridge, UK, 1997.
32. He, H.; Kim, K.H.; Danilov, A.; Montemurro, D.; Yu, L.; Park, Y.W.; Lombardi, F.; Bauch, T.; Moth-Poulsen, K.; Iakimov, T.; Yakimova, R.; Malmberg, P.; Müller, C.; Kubatkin, S.; Lara-Avila, S. Uniform doping of graphene close to the Dirac point by polymer-assisted assembly of molecular dopants. *Nat. Commun.* **2018**, *9*, 3956. https://doi.org/10.1038/s41467-018-06352-5.
33. Yager, T.; Lartsev, A.; Cedergren, K.; Yakimova, R.; Panchal, V.; Kazakova, O.; Tzalenchuk, A.; Kim, K.-H.; Park, Y.-W.; Lara-Avila, S.; Kubatkin, S. Low contact resistance in epitaxial graphene devices for quantum metrology. *AIP Adv*. 2015, *5*, 087134. https://doi.org/10.1063/1.4928653.